Weak- and strong-coupling electrostatic interactions between asymmetrically charged planar surfaces

M. Kanduč,[1] M. Trulsson,[2] A. Naji,[3,4] Y. Burak,[5] J. Forsman,[2] and R. Podgornik[1,4,6,7]

[1]*Department of Theoretical Physics, J. Stefan Institute, SI-1000 Ljubljana, Slovenia*

[2]*Department of Theoretical Chemistry, Lund University Chemical Center, P.O. Box 124, S-221 00 Lund, Sweden*

[3]*Materials Research Laboratory, and Department of Chemistry and Biochemistry, University of California,
Santa Barbara, California 93106, USA*

[4]*Kavli Institute for Theoretical Physics, University of California, Santa Barbara, California 93106, USA*

[5]*Center for Brain Science, Harvard University, Cambridge, Massachusetts 02138, USA*

[6]*Department of Physics, Faculty of Mathematics and Physics, University of Ljubljana, SI-1000 Ljubljana, Slovenia*

[7]*Laboratory of Physical and Structural Biology, NICHD, Bld. 9, Rm. 1E116, National Institutes of Health,
Bethesda, Maryland 20892-0924, USA*

(Received 27 August 2008; published 5 December 2008)

We compare weak- and strong-coupling theory of counterion-mediated electrostatic interactions between two asymmetrically charged plates with extensive Monte Carlo simulations. Analytical results in both weak- and strong-coupling limits compare excellently with simulations in their respective regimes of validity. The system shows a surprisingly rich structure in terms of interactions between the surfaces as well as fundamental qualitative differences in behavior in the weak- and the strong-coupling limits.

PACS number(s): 05.20.Jj, 61.20.Qg

I. INTRODUCTION

Stability and interactions in biological and soft-matter systems often depends on the underlying properties of electrostatic interactions [1]. Charges on macromolecular surfaces in aqueous environments, as in the case of membranes, self-assembled micelles, globular proteins, and fibrous polysaccharides, affect a wealth of functional, structural, and dynamical properties [2]. The traditional approach to charged (bio)colloidal systems has been the mean-field Poisson-Boltzmann (PB) formalism applicable at weak surface charges, low counterion valency, and high temperature [3]. The limitations of this approach become practically important in highly charged systems where counterion-mediated interactions between charged bodies start to deviate substantially from the mean-field accepted wisdom [4,5]. One of the fundamental recent advances in this field has been the systematization of these non-PB effects based on the notions of weak- and strong-coupling approximations. The latter approach has been pioneered by Rouzina and Bloomfield [6], elaborated later by Shklovskii *et al.* [7], Levin *et al.* [8], and brought into final form by Netz *et al.* [4,5,9]. These two approximations allow for an explicit and exact treatment of charged systems at two disjoint limiting conditions whereas the parameter space in between can be analyzed only approximately [9–12,17] and is mostly accessible solely *via* computer simulations [4,5,9,13–19].

In the absence of a general approach that would cover thoroughly all the regions of the parameter space one must take recourse to various partial formulations that take into account only this or that facet of the problem. In this respect the counterion-only or the one-component Coulomb fluid model system has proved to be of substantial value [4]. Heuristically as well as numerically. A proper understanding of the behavior of charged systems would thus start with the analysis of counterion distribution around charged macromo-lecular surfaces, neglecting completely the effects of salt.

Both the weak- and the strong-coupling approximations are based on a functional integral or field-theoretic representation [20] of the grand canonical partition function of a system composed of fixed surface charges with intervening mobile counterions, and depend on the value of a single dimensionless coupling parameter Ξ [9]. The distance at which two unit charges interact with thermal energy $k_\mathrm{B}T$ is known as the Bjerrum length $\ell_\mathrm{B} = e_0^2/(4\pi\varepsilon\varepsilon_0 k_\mathrm{B}T)$ (in water at room temperature, one has $\ell_\mathrm{B} \simeq 0.7$ nm). If the charge valency of the counterions is q then the aforementioned distance scales as $q^2\ell_\mathrm{B}$. Similarly, the distance at which a counterion interacts with a macromolecular surface (of surface charge density σ) with an energy equal to $k_\mathrm{B}T$ is called the Gouy-Chapman length, defined as $\mu = e_0/(2\pi q\ell_\mathrm{B}\sigma)$. A competition between ion-ion and ion-surface interactions can be quantitatively measured with a ratio of these characteristic lengths, that is $\Xi = q^2\ell_\mathrm{B}/\mu = 2\pi q^3\ell_\mathrm{B}^2\sigma/e_0$, which is known as the (Netz-Moreira) electrostatic coupling parameter [9]. The weak-coupling (WC) regime $\Xi \ll 1$ (appropriate for low valency counterions and/or weakly charged surfaces) is characterized by the fact that the width of the counterion layer μ is much larger than the separation between two neighboring counterions in solution and thus the counterion layer behaves basically as a three-dimensional gas. Each counterion in this case interacts with many others and the collective mean-field approach of the Poisson-Boltzmann (PB) type is completely justified. On the other hand, in the strong-coupling (SC) regime $\Xi \gg 1$ (appropriate for high valency counterions and/or highly charged surfaces), the mean distance between counterions, $a_\perp = \sigma/qe_0$, is much larger than the layer width (i.e., $a_\perp/\mu \sim \sqrt{\Xi} \gg 1$), indicating that the counterions are highly localized laterally and form a strongly correlated quasi-two-dimensional layer next to a charged surface. In this case, the weak-coupling approach breaks down due to strong counterion-surface and counterion-counterion correlations.

Since counterions can move almost independently from the others along the direction perpendicular to the surface, the collective many-body effects that enable a mean-field description are absent, necessitating a complementary SC description [9]. The range of validity of both limiting theories at intermediate values of the coupling parameter has been explored thoroughly in the literature [4,5,9–12,17].

Formally the weak-coupling limit can be straightforwardly identified with the saddle-point approximation of the field theoretic representation of the grand canonical partition function, and is reduced to the mean-field PB theory in the lowest order for $\Xi \to 0$. The quadratic fluctuations around the mean field provide a second-order correction to the mean-field solution for small finite $\Xi < 1$ [20–26]. The strong-coupling approximation has no PB-like correlates [9] since it is formally equivalent to a single particle description obtained from a systematic $1/\Xi$ expansion in the limit $\Xi \to \infty$, and corresponds to two lowest-order terms in the virial expansion of the grand canonical partition function. The consequences and the formalism of these two limits of the Coulomb fluid description have been explored widely and in detail (for reviews, see Refs. [4,5]).

Considering the inhomogeneity of charged surfaces in various biological contexts it has always been of interest to investigate not just electrostatic interactions between symmetrical charged surfaces, i.e., those bearing equal charges of the same sign, but also interactions between surfaces bearing unequal charges or even charges of opposite sign [19,27–32]. This problem has a venerable history starting from the seminal work of Parsegian and Gingell [27] who formulated a linearized PB theory of the interactions in the presence of salt. The linearization *ansatz* was later generalized in the work of Lau and Pincus [28] and Ben-Yaakov *et al.* [29] who formulated the appropriate nonlinear mean-field theory of nonsymmetric electrostatic interactions.

It is thus our goal in this contribution to show how and to what extent the asymmetry in the distribution of charges on two apposed planar surfaces affects the interactions between macromolecular surfaces carrying them. Below we shall present a complete analysis of the asymmetric case in the weak-coupling limit, i.e., the mean-field Poisson-Boltzmann theory supplemented with a quadratic-fluctuations analysis, as well as in the strong-coupling limit *via* the asymptotic strong-coupling theory and evaluate how these analytical results compare with extensive numerical simulations. We will show that in their respective regimes of validity (i.e., small and/or large couplings) both approximations present a very accurate quantitative statistical description of the system.

II. GEOMETRY

In our model system we consider uniform surface charge distributions on two plane-parallel surfaces (located at $z = \pm a$) given by the surface charge density of the form

$$\rho_0(\mathbf{r}) = \sigma_1 \delta(z+a) + \sigma_2 \delta(z-a). \quad (1)$$

We may interchangeably use the half-separation a, or

$$D = 2a \quad (2)$$
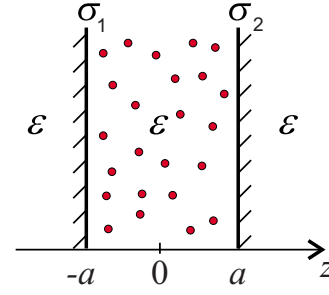
to identify the surface-surface distance.

FIG. 1. (Color online) Geometry of the system comprising two asymmetrically charged planar surfaces located at $z = \pm a$ (at separation distance $D = 2a$) with neutralizing pointlike counterions of valency q distributed in between [33].

We assume furthermore that the charge of both bounding surfaces is compensated by mobile counterions of charge valency q immersed in an aqueous medium of dielectric constant ε and distributed in between the two surfaces (see Fig. 1). We thus neglect all coions. This approximation is relevant for low salt concentrations where the Debye screening length is much larger than the scales of interest [34]. We consider the surfaces as impenetrable to counterions and neglect the dielectric discontinuity across the bounding surfaces which was addressed at various levels of approximation in [35–38].

Without loss of generality we can assume here that $q > 0$ and

$$\sigma_1 + \sigma_2 < 0 \quad \text{and} \quad \sigma_2 > \sigma_1, \quad \text{so that} \quad \sigma_1 < 0. \quad (3)$$

It will be helpful for our later developments to introduce an asymmetry parameter ζ that will allow us to quantify the dissimilarity between the two bounding surfaces as

$$\zeta = \frac{\sigma_2}{\sigma_1} > -1. \quad (4)$$

Furthermore, by suitably normalizing the results one can concentrate exclusively on the interval $-1 \leq \zeta \leq 1$. All other cases can be mapped onto this interval with appropriate rescaling of the parameters. The values $\zeta = 1$ and $\zeta = -1$ represent exceptional points in the parameter space: $\zeta = 1$ is the standard symmetric case ($\sigma_1 = \sigma_2$) already amply treated in the literature, and $\zeta = -1$ represents the antisymmetric case ($\sigma_1 = -\sigma_2$) with no counterions between surfaces that reduces to the trivial case of a planar capacitor. These two well-understood limiting cases will be thus omitted from our discussion.

Counterions between the surfaces satisfy the electroneutrality condition that can be written in the form

$$N e_0 q + (\sigma_1 + \sigma_2) S = 0, \quad (5)$$

where S denotes the (infinite) area of each surface.

III. DIMENSIONLESS REPRESENTATION

Because of the asymmetry present in the system, we have two length scales describing the interaction of the counterions with each of the bounding surfaces. These two length scales are given by the corresponding Gouy-Chapman lengths associated with the two surfaces as

$$\mu_1 = \frac{e_0}{2\pi\ell_B q|\sigma_1|} \equiv \mu, \quad \mu_2 = \frac{e_0}{2\pi\ell_B q|\sigma_2|} = \frac{\mu}{|\zeta|}. \quad (6)$$

For the same reason we can thus define two different coupling parameters

$$\Xi_1 = \frac{q^2\ell_B}{\mu_1} \equiv \Xi, \quad \Xi_2 = \frac{q^2\ell_B}{\mu_2} = |\zeta|\Xi, \quad (7)$$

each one being defined by the ratio between the Bjerrum length and the corresponding Gouy-Chapman length. In what follows, we rescale the surface separation as

$$\widetilde{D} = D/\mu \quad (8)$$

(or the rescaled half-distance as $\widetilde{a} = a/\mu$) with respect to plate 1. With an appropriate rescaling one could also equivalently define all dimensionless lengths with respect to plate 2. Thus, the minimal set of dimensionless parameters that fully characterize the system in the thermodynamic limit is given by $\{\Xi, \zeta, \widetilde{D}\}$.

Other physical quantities such as the mean electrostatic potential $\psi(z)$, number density of counterions, $n(z)$, and the pressure, p, acting on each surface can be rescaled as well. We shall use the standard rescaled electrostatic potential

$$\widetilde{\psi}(z) = \beta q e_0 \psi(z),$$

as well as the rescaled density and pressure

$$\widetilde{n}(z) = \frac{n(z)}{2\pi\ell_B(\sigma_1/e_0)^2} \quad \text{and} \quad \widetilde{p} = \frac{\beta p}{2\pi\ell_B(\sigma_1/e_0)^2}, \quad (9)$$

where $\beta = 1/k_B T$, and all the other quantities have been defined above.

IV. MEAN-FIELD POISSON-BOLTZMANN APPROXIMATION

In the weak-coupling regime, the leading contribution to the partition function comes from the saddle-point configuration of the local fluctuating electrostatic potential, $\psi_0(z)$ [20]. The saddle-point configuration can be straightforwardly translated into a solution of the PB equation and corresponds to an exact asymptotic result in the limit $\Xi \to 0$ [9,23]. For a system containing only counterions, the PB equation for the dimensionless potential, $\widetilde{\psi}_0(z)$, can be written in the standard form [2,3]

$$\frac{d^2\widetilde{\psi}_0(z)}{dz^2} = -(4\pi\ell_B q^2)\lambda_0 e^{-\widetilde{\psi}_0(z)}, \quad (10)$$

with boundary conditions

$$\left.\frac{d\widetilde{\psi}_0}{dz}\right|_{-a} = \frac{2}{\mu},$$

$$\left.\frac{d\widetilde{\psi}_0}{dz}\right|_{a} = -\frac{2\zeta}{\mu}. \quad (11)$$

Integration of the PB equation gives rise to the first integral of the system of the form

$$\beta p_0 = -\frac{1}{8\pi\ell_B q^2}\left(\frac{d\widetilde{\psi}_0}{dz}\right)^2 + n_0(z), \quad (12)$$

where the constant p_0 is nothing but the mean-field PB pressure acting between the bounding surfaces [2] and

$$n_0(z) = \lambda_0 e^{-\widetilde{\psi}_0(z)}, \quad (13)$$

is the PB number density profile of counterions between the surfaces. The normalization factor λ_0 follows from the electroneutrality condition (5) as

$$\lambda_0 = -\frac{\sigma_1 + \sigma_2}{q e_0 \displaystyle\int_{-a}^{a} dz\, e^{-\widetilde{\psi}_0(z)}}. \quad (14)$$

The nature of the solution $\widetilde{\psi}_0(z)$ obviously crucially depends on the sign of the pressure p_0 [28,29]. Different forms are obtained for positive and negative pressures, corresponding to repulsion and attraction between the bounding surfaces, respectively. We review these different cases separately.

A. Repulsion regime $p_0 > 0$

In the case of repulsive pressure the appropriate solution of Eq. (10) can be written as

$$\widetilde{\psi}_0 = \ln\left(\frac{\lambda_0}{\beta p_0}\cos^2 \alpha(z - z_0)\right), \quad (15)$$

where the constants z_0 and $\alpha^2 \equiv 2\pi\ell_B q^2(\beta p_0)$ are obtained from the boundary conditions (11) and satisfy the set of two equations

$$\alpha \tan \alpha(a + z_0) = \frac{1}{\mu}, \quad (16)$$

$$\alpha \tan \alpha(a - z_0) = \frac{\zeta}{\mu}. \quad (17)$$

Eliminating z_0 we obtain an equation for α of the form

$$\tan(2\alpha a) = \frac{\alpha(\zeta + 1)\mu}{\alpha^2\mu^2 - \zeta}. \quad (18)$$

The solution of this equation provides the final result for the repulsive PB pressure p_0. Note in particular that in rescaled units and by definition one has

$$\widetilde{p}_0 = \widetilde{\alpha}^2, \quad (19)$$

where $\widetilde{\alpha} = \alpha\mu$. Once α is known, the parameter z_0 can be simply obtained from Eqs. (16) or (17) and thus the potential $\widetilde{\psi}_0(z)$, Eq. (15), is fully determined. The density profile of counterions then follows from

$$n_0(z) = \frac{\beta p_0}{\cos^2 \alpha(z - z_0)}. \quad (20)$$

A positive (repulsive) solution for the pressure as considered in this section is always possible for any given asym-

metry parameter ζ (excluding the trivial case of $\zeta = -1$). In particular, it easily follows that within the mean-field theory two surfaces of equal sign ($\zeta > 0$) always repel, that is at all separation distances $\widetilde{D}$. When the surfaces bear charges of opposite sign $\zeta < 0$, they attract at large separations (see below) and a repulsion emerges only at sufficiently small separations.

At small separations $\widetilde{D} \ll 1$, we can obtain the limiting solution for α and thus the limiting small-distance pressure p_0 as

$$\widetilde{p}_0(\widetilde{D}) \simeq \frac{1 + \zeta}{\widetilde{D}} \tag{21}$$

for arbitrary $|\zeta| < 1$ as noted in Sec. II. This is of course nothing but the ideal-gas osmotic pressure of counterion confined between the two plates [i.e., $p_0 = N k_B T/(SD)$ in actual units], which dominates over the energetic contributions at small separations. At large separations $\widetilde{D} \gg 1$ and for $\zeta > 0$, we obtain the asymptotic expansion

$$\widetilde{p}_0(\widetilde{D}) = \frac{\pi^2}{\widetilde{D}^2} \left[1 - \frac{2(\zeta + 1)}{\zeta \widetilde{D}} + O\left(\frac{1}{\widetilde{D}^2} \right) \right], \tag{22}$$

which is valid for $\widetilde{D} \gg 2(1 + 1/\zeta)$. Thus, in the limit $\widetilde{D} \to \infty$, the pressure behaves as

$$\widetilde{p}_0(\widetilde{D}) \simeq \frac{\pi^2}{\widetilde{D}^2}, \tag{23}$$

which agrees with the asymptotic pressure between two equally charged surfaces ($\zeta = 1$). For smaller ζ than determined above, i.e., for $\zeta^{-1} \gg \widetilde{D} \gg 1$, one needs to invoke a different asymptotic expansion and specifically for $\zeta \simeq 0$ (one surface being neutral), one obtains

$$\widetilde{p}_0(\widetilde{D}) \simeq \frac{\pi^2}{4 \widetilde{D}^2}. \tag{24}$$

This latter asymptotic result may be obtained from the one in Eq. (23) by redefining $\widetilde{D} \to 2\widetilde{D}$. This may be understood simply by noting that because of symmetry a system with $\zeta > 0$ may be decomposed into two halves each with an effective asymmetry parameter $\zeta = 0$.

B. Attraction regime $p_0 < 0$

An attractive pressure on the mean-field level is possible only if the surfaces are oppositely charged $\zeta < 0$. The appropriate solution in this case is given by

$$\widetilde{\psi}_0 = \ln \left(\frac{\lambda_0}{\beta |p_0|} \sinh^2 \alpha(z - z_0) \right), \tag{25}$$

where the constants z_0 and $\alpha^2 \equiv 2\pi \ell_B q^2 (\beta |p_0|)$ can again be obtained from boundary conditions, this time in the form

$$\alpha \coth \alpha(a + z_0) = -\frac{1}{\mu}, \tag{26}$$

$$\alpha \coth \alpha(a - z_0) = -\frac{\zeta}{\mu}. \tag{27}$$

Eliminating z_0 we obtain an equation for α as

$$\coth(2\alpha a) = -\frac{\zeta + \mu^2 \alpha^2}{\mu \alpha (1 + \zeta)}. \tag{28}$$

In this case we have in rescaled units

$$\widetilde{p}_0 = -\widetilde{\alpha}^2, \tag{29}$$

and for the density profile of counterions

$$n_0(z) = \frac{\beta |p_0|}{\sinh^2 \alpha(z - z_0)}. \tag{30}$$

The asymptotic form of the attractive pressure at large separations $\widetilde{D} \gg 1$ can be derived as

$$\widetilde{p}_0(\widetilde{D}) \simeq -\zeta^2 \left(1 - 4 \frac{1 + \zeta}{1 - \zeta} e^{2\zeta \widetilde{D}} \right), \tag{31}$$

where $\zeta < 0$ as noted above. For infinite separations, this pressure does not vanish and exponentially approaches $-\zeta^2$ since for $\zeta < 0$ the system behaves partially as a simple capacitor.

C. Zero pressure $p_0 = 0$

In the case of charged surfaces with opposite sign ($\zeta < 0$), the large-distance attraction regime and the short-distance repulsion regime merge at the point of zero pressure, $\widetilde{D} = \widetilde{D}^*$, where the surfaces are at equilibrium. In this case, the PB solution for the potential reads as

$$\widetilde{\psi}_0 = \ln[2\pi \ell_B q^2 \lambda_0 (z - z_0)^2], \tag{32}$$

and the density profile of counterions is given by

$$n_0(z) = \frac{1}{2\pi \ell_B q^2 (z - z_0)^2}, \tag{33}$$

where z_0 is found from the boundary conditions as $z_0 = -\mu - D^*/2$, and the bound-state separation, D^*, follows in rescaled units as

$$\widetilde{D}^* = -\frac{1 + \zeta}{\zeta}. \tag{34}$$

The surfaces attract for $\widetilde{D} > \widetilde{D}^*$ and repel for $\widetilde{D} < \widetilde{D}^*$. In the vicinity of $\widetilde{D}^*$, that is for $|\widetilde{D}^* - \widetilde{D}| \ll 1$, the pressure behaves as

$$\widetilde{p}_0 \simeq \frac{3\zeta^3}{1 + \zeta^3} |\widetilde{D}^* - \widetilde{D}|. \tag{35}$$

This concludes the calculation of the intersurface pressure on the mean-field PB level strictly valid for $\Xi \to 0$.

The preceding results may be summarized in a phase diagram shown in Fig. 4 in terms of D^* and the asymmetry parameter ζ displaying the mean-field attraction and repulsion regimes separated by the boundary line (34). The forms

of the pressure here are completely consistent with those derived by Lau and Pincus [28] *via* a different route.

V. WEAK-COUPLING ANALYSIS: QUADRATIC FLUCTUATIONS AROUND MEAN FIELD

The first nonzero correction to the saddle point is second order in the fluctuations of the local electrostatic potential around the mean-field PB solution, ψ_0. Our goal here is to calculate the corrections in pressure, $p_2(D)$, stemming from these quadratic fluctuations, which leads then to the total WC pressure,

$$p(D) = p_0(D) + p_2(D). \quad (36)$$

This approach has correlates in many diverse areas of physics where fluctuations around a mean-field solution are important [39] and goes under different names, though the physics is always the same. We may conventionally refer to the mean-field PB term, $p_0(D)$, and the fluctuations contribution, $p_2(D)$, as the zeroth-order and the second-order correction terms on the WC level, respectively. This procedure formally also corresponds to a series expansion in powers of Ξ (loop expansion) around the asymptotic mean-field solution ($\Xi \to 0$) [9,20,23,36] and is thus expected to be valid for sufficiently small coupling parameters as will be determined later. Note also that in this latter sense the second-order pressure turns out to be proportional to Ξ, that is $p_2 \sim \Xi$, and thus corresponds to a first-loop correction [9,23].

In order to proceed, one needs to evaluate the appropriate Hessian of the field action in the partition function and study its fluctuation spectrum (see Refs. [20,36] for more details). The Hessian of the field action can be derived in the form

$$H(\mathbf{r}, \mathbf{r}') = u^{-1}(\mathbf{r}, \mathbf{r}') + \beta(e_0 q)^2 n_0(z) \delta^3(\mathbf{r} - \mathbf{r}'), \quad (37)$$

where $u^{-1}(\mathbf{r}, \mathbf{r}') = -\varepsilon\varepsilon_0 \nabla_{\mathbf{r}}^2 \delta^3(\mathbf{r} - \mathbf{r}')$ is the inverse Coulomb operator and $n_0(z)$ is the zeroth-order PB density as derived in the preceding section. Hence,

$$(4\pi\ell_B q^2) n_0(z) = \begin{cases} \dfrac{2\alpha^2}{\cos^2 \alpha(z - z_0)}, & p_0 > 0, \\[3mm] \dfrac{2}{(z - z_0)^2}, & p_0 = 0, \\[3mm] \dfrac{2\alpha^2}{\sinh^2 \alpha(z - z_0)}, & p_0 < 0. \end{cases} \quad (38)$$

The corresponding correction, $\mathcal{F}_2$, to the free energy of the system is then given by the trace-log of the Hessian. It can be written equivalently in the following form [20,21]:

$$\beta\mathcal{F}_2 = \frac{1}{2}\text{Tr} \ln H(\mathbf{r}, \mathbf{r}') = \frac{S}{4\pi}\int_0^\infty Q \ln \frac{\mathcal{D}_1(Q)}{\mathcal{D}_0(Q)} dQ. \quad (39)$$

This form can be derived rather straightforwardly by using the argument principle [21] and converting the discrete sum of eigenvalues of the Hessian operator into an integral over the transverse wave vector $\mathbf{Q} = (Q_x, Q_y)$, with density of modes $S/(2\pi)^2$ of the logarithm of the secular determinant

$\mathcal{D}_\lambda$ of the same operator. The index λ in the secular determinant refers to the eigenvalue equation that can be derived in the form

$$\left(\frac{\partial^2}{\partial z^2} - Q^2 - \lambda(4\pi\ell_B q^2)n_0(z)\right)f_\lambda(\mathbf{Q}, z) = 0. \quad (40)$$

By simply writing $\mathcal{D}(a, Q)$ for the quotient $\mathcal{D}_1(Q)/\mathcal{D}_0(Q)$, and noting that the secular determinant depends explicitly also on the value of the intersurface spacing, a, the free energy contribution from the quadratic fluctuations can be equivalently expressed exactly in a dimensionless form as

$$\frac{\tilde{\mathcal{F}}_2}{\tilde{S}} = \frac{1}{2}\Xi \int_0^\infty \tilde{Q} \ln \mathcal{D}(\tilde{a}, \tilde{Q}) d\tilde{Q}, \quad (41)$$

where $\tilde{\mathcal{F}}_2 = 2\varepsilon\varepsilon_0 \mathcal{F}_2 / \sigma_1^2 \mu^3$, $\tilde{Q} = \mu Q$, and the rescaled area $\tilde{S} = S/\mu^2$. Here the secular determinant of the Hessian for homogeneous transverse modes has been written as a function of dimensionless quantities $\tilde{a} = a/\mu$, $\tilde{Q} = \mu Q$. This determinant must be standardly regularized so that all irrelevant constants, i.e., all the terms not depending on the separation between the bounding surfaces, are dropped, amounting to a rescaling

$$\mathcal{D}(\tilde{a}, \tilde{Q}) \to \frac{\mathcal{D}(\tilde{a}, \tilde{Q})}{\mathcal{D}(\tilde{a} \to \infty, \tilde{Q})}. \quad (42)$$

This corresponds to a subtraction of the part of the free energy for two separate interfaces at infinite separation from the total free energy.

In the next step one must calculate the secular determinant $\mathcal{D}(\tilde{a}, \tilde{Q})$ for each of the pressure regimes separately, since the appropriate eigenfunctions of the Hessian depend on the mean-field solution that in its turn depends on the sign of the interaction pressure, see Eq. (38). In what follows we shall follow closely the derivations in Refs. [20,21,36].

The total pressure in the weak-coupling limit is the sum of the PB pressure and the quadratic fluctuations correction. It can be written as

$$\tilde{p}(\tilde{D}) = \tilde{p}_0(\tilde{D}) + \tilde{p}_2(\tilde{D}) = \tilde{p}_0(\tilde{D}) - \frac{1}{\tilde{S}}\left\langle \frac{\partial \tilde{\mathcal{F}}_2}{\partial \tilde{D}} \right\rangle. \quad (43)$$

A. Repulsion regime $p_0 > 0$

In this regime the secular determinant of the Hessian, Eq. (40), can be obtained by solving

$$\left(\frac{d^2}{dz^2} - Q^2 - \frac{2\alpha^2}{\cos^2 \alpha(z - z_0)}\right)y(Q, z) = 0, \quad (44)$$

with appropriate boundary conditions implying continuity of the solution and its derivative across the bounding surfaces at $z = \pm a$.

The general solution of Eq. (44) for various regions in the perpendicular direction can be written in the form

$$y(Q,z) = \begin{cases} Ae^{Qz}, & z < -a, \\ By_1 + Cy_2, & -a < z < a, \\ De^{-Qz}, & z > a, \end{cases} \qquad (45)$$

where

$$y_1 = e^{Qz}\left(1 + \frac{\alpha}{Q}\tan\alpha(z - z_0)\right), \qquad (46)$$

$$y_2 = \frac{Q^2}{Q^2 + \alpha^2}e^{-Qz}\left(1 - \frac{\alpha}{Q}\tan\alpha(z - z_0)\right). \qquad (47)$$

Taking into account the continuity of the solution and its derivatives we get a set of four homogeneous equations for the coefficients A, B, C, and D. The solution exists only if the (secular) determinant of this system equals zero. Thus, we derive the secular determinant of the Hessian operator in this case in the rescaled form

$$\mathcal{D}(\tilde{a}, \tilde{Q}) = \frac{\Gamma_+(\tilde{\alpha}, \tilde{Q}) - \Gamma_+(\tilde{\alpha}, 0)e^{-4\tilde{Q}\tilde{a}}}{\tilde{Q}^2 + \tilde{\alpha}^2}, \qquad (48)$$

where

$$\Gamma_+(\tilde{\alpha}, \tilde{Q}) = (1 + \tilde{\alpha}^2 + 2\tilde{Q} + 2\tilde{Q}^2)(\zeta^2 + \tilde{\alpha}^2 + 2\zeta\tilde{Q} + 2\tilde{Q}^2). \qquad (49)$$

The regularized form of the secular determinant is obtained by taking the quotient as indicated in Eq. (42). While doing this, it is important to realize that $\tilde{\alpha}$ also depends on the intersurface distance. In fact from Eq. (23) it follows that the appropriate limit of $\tilde{\alpha}$ is

$$\lim_{\tilde{a} \to \infty} \tilde{\alpha}(\tilde{a}) = 0. \qquad (50)$$

In the regularization of the secular determinant this limiting behavior should be consistently taken into account.

Finally, the dimensionless quadratic fluctuations free energy $\tilde{\mathcal{F}}_2$ can be calculated numerically *via* Eqs. (41) and (48). The fluctuations contribution to the pressure, $\tilde{p}_2$, then follows from Eq. (43).

The asymptotic form of the second-order dimensionless pressure can be obtained analytically. Note that at large separations $\tilde{D} \to \infty$, a repulsive mean-field pressure $p_0 > 0$, as considered in this section, is possible only for non-negative ζ. For not too small $\zeta > 0$, i.e., when $\tilde{D} \gg 2(1 + 1/\zeta)$, we find

$$\tilde{p}_2(\tilde{D}) \simeq -\Xi\pi^2\frac{\ln\tilde{D}}{\tilde{D}^3}, \qquad (51)$$

while for $\zeta \simeq 0$, i.e., when $\zeta^{-1} \gg \tilde{D} \gg 1$, we get

$$\tilde{p}_2(\tilde{D}) \simeq -\Xi\pi^2\frac{\ln\tilde{D}}{8\tilde{D}^3}. \qquad (52)$$

Again the difference in the two cases above is due to the symmetry of the problem in the latter case, that can be de-

scribed by redefining $\tilde{D} \to 2\tilde{D}$ and discarding the subdominant terms.

The second-order pressure is obviously attractive and in this regime leads to a reduction of the total pressure from the mean-field value p_0. This clearly shows that electrostatic correlations favor attraction between two repelling asymmetrically charged plates. However, the total pressure never becomes negative as the fluctuations are assumed to be small within the second-order weak-coupling analysis.

B. Attraction regime $p_0 < 0$

In this case the secular determinant of the Hessian, Eq. (40), is obtained by solving

$$\left(\frac{d^2}{dz^2} - Q^2 - \frac{2\alpha^2}{\sinh^2\alpha(z - z_0)}\right)y(Q,z) = 0. \qquad (53)$$

The general solutions for particular regions in the z direction are

$$y(Q,z) = \begin{cases} Ee^{Qz}, & z < -a, \\ Fy_1 + Gy_2, & -a < z < a, \\ He^{-Qz}, & z > a, \end{cases} \qquad (54)$$

where

$$y_1 = e^{Qz}\left(1 - \frac{\alpha}{Q}\coth\alpha(z - z_0)\right), \qquad (55)$$

$$y_2 = \frac{Q^2}{Q^2 - \alpha^2}e^{-Qz}\left(1 + \frac{\alpha}{Q}\coth\alpha(z - z_0)\right). \qquad (56)$$

Again the solution exists only if the determinant of the system of equations, which connect coefficients E, F, G, H and stems from the application of the boundary conditions at $z = \pm a$, is identically zero. This again defines the secular determinant $\mathcal{D}(a, Q)$ appropriate for this case. It is easy to show that the secular determinant $\mathcal{D}(a, Q)$ can be obtained from the $p_0 > 0$ result, Eq. (48), simply by substituting $\alpha^2 \to -\alpha^2$ and so we can write

$$\mathcal{D}(\tilde{a}, \tilde{Q}) = \frac{\Gamma_-(\tilde{\alpha}, \tilde{Q}) - \Gamma_-(\tilde{\alpha}, 0)e^{-4\tilde{Q}\tilde{a}}}{\tilde{Q}^2 - \tilde{\alpha}^2}, \qquad (57)$$

where

$$\Gamma_-(\tilde{\alpha}, \tilde{Q}) = (1 - \tilde{\alpha}^2 + 2\tilde{Q} + 2\tilde{Q}^2)(\zeta^2 - \tilde{\alpha}^2 + 2\zeta\tilde{Q} + 2\tilde{Q}^2). \qquad (58)$$

Here we can again regularize the secular determinant to discard divergences, Eq. (42). Again one must be careful by taking the correct limit for $\tilde{\alpha}$ in the above regularization scheme. In this regime, the appropriate limit is given by

$$\lim_{\tilde{a} \to \infty} \tilde{\alpha}(\tilde{a}) = -\zeta, \qquad (59)$$

as follows straightforwardly from Eq. (31). The fluctuations contribution to the pressure, $\tilde{p}_2$, can then be evaluated numerically from Eq. (43).
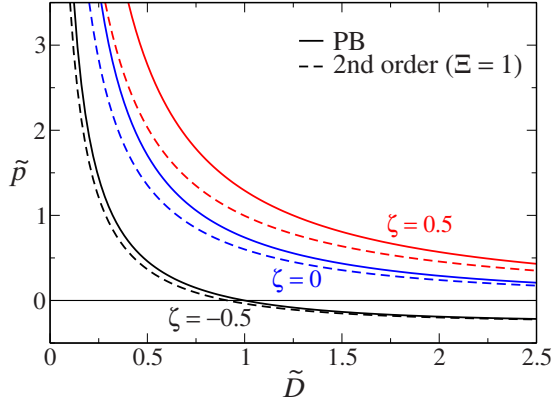
FIG. 2. (Color online) Rescaled weak-coupling intersurface pressure, Eqs. (19) and (29), as a function of the rescaled distance, $\tilde{D}$, between two charged plates for three different asymmetry parameters $\zeta = -0.5$, 0, and 0.5 as shown on the graph. The total pressure, $\tilde{p} = \tilde{p}_0 + \tilde{p}_2$ [dashed lines, plotted here for $\Xi = 1$ using Eq. (43)], is always lowered from its mean-field PB value, p_0 (solid lines, obtained for $\Xi \to 0$), since quadratic fluctuations around mean field favor attraction.

The asymptotic form of $\tilde{p}_2$ for $\tilde{D} \gg 1$ can be derived analytically as

$$\tilde{p}_2(\tilde{D}) \simeq \Xi f(\zeta) e^{2\zeta \tilde{D}}, \tag{60}$$

which is applicable only for charged surfaces of opposite sign, $\zeta < 0$, which can attract ($p_0 < 0$) at large separations. The function $f(\zeta)$ is defined as

$$f(\zeta) = \zeta^3 \frac{1+\zeta}{1-\zeta} \left(\frac{2 \arctan \sqrt{1-2\zeta^2}}{\sqrt{1-2\zeta^2}} + \ln \frac{1-\zeta^2}{2\zeta^2} \right) \tag{61}$$

for $-\sqrt{2}/2 < \zeta < 0$, and

$$f(\zeta) = \zeta^3 \frac{1+\zeta}{1-\zeta} \left(\frac{2 \tanh^{-1} \sqrt{2\zeta^2-1}}{\sqrt{2\zeta^2-1}} + \ln \frac{1-\zeta^2}{2\zeta^2} \right) \tag{62}$$

for $-1 < \zeta < -\sqrt{2}/2$. The second-order pressure thus asymptotically decays exponentially and can be only attractive. For not too small values of ζ, it is thus qualitatively very different from the case $\zeta \geq 0$.

The total weak-coupling pressure, $\tilde{p} = \tilde{p}_0 + \tilde{p}_2$, is shown in Fig. 2 for a few different asymmetry parameters and a relatively small value of the coupling parameter Ξ.

C. Regime of validity of the weak-coupling theory

As noted above the foregoing weak-coupling analysis is valid as long as the quadratic corrections are sufficiently small so that the series expansion around the mean-field solution does not diverge [9,23]. As an approximate measure for the validity regime of this scheme, one can require that the second-order correction term is smaller than the leading order term, i.e.,

$$|\tilde{p}_2| < |\tilde{p}_0|. \tag{63}$$

This leads to a useful criterion identifying the regime of coupling parameters and distances in which the weak-coupling

theory is applicable. For $p_0 > 0$ and by employing the closed-form expressions obtained for large separations $\tilde{D} \gg 1$, we find the validity condition

$$\Xi < \frac{\tilde{D}}{\ln \tilde{D}}. \tag{64}$$

This indicates that at a given nonvanishing Ξ, the weak-coupling scheme becomes increasingly more accurate at larger separations, while as the surfaces get closer a smaller coupling parameter needs to be chosen.

On the other hand, for $p_0 < 0$ (which occurs for $\zeta < 0$) and at large separations $\tilde{D} \gg 1$, we obtain

$$\Xi < \frac{\zeta^2}{|f(\zeta)|} e^{-2\zeta \tilde{D}}. \tag{65}$$

The right-hand side here is exponentially large meaning that for charged surfaces of opposite sign, the weak-coupling analysis performs far better at finite coupling parameters and smaller intersurface separations than for the surfaces of equal sign ($\zeta > 0$).

Finally, note that for $p_0 = 0$ that corresponds to the equilibrium phase boundary line in Fig. 4 for $\zeta < 0$, we deal with a situation where the leading order term is zero and the fluctuations are dominant at any finite value of Ξ. The convergence of the loop expansion must be determined in this case by evaluating the higher-order terms which we shall not consider in this paper.

VI. STRONG-COUPLING THEORY

The strong-coupling approximation coincides with the lowest-order nontrivial expansion of the partition function in terms of the fugacities of the counterions. This expansion may be expressed as a $1/\Xi$ series expansion [9], whose leading order term ($\Xi \to \infty$) corresponds to the so-called SC theory. We will not delve into the strong-coupling expansion in more detail since it has been exhaustively reviewed in the literature [4,5,9]. On the leading order, the free energy is obtained as

$$\mathcal{F} = W_0 - N k_B T \ln \int e^{-\beta(W_1+W_2)} dV, \tag{66}$$

where W_0 is electrostatic interaction energy of charged surfaces

$$W_0 = \frac{\sigma_1 \sigma_2}{2\varepsilon\varepsilon_0} SD, \tag{67}$$

with S representing surface area of each plate, and W_1 and W_2 are electrostatic interaction energies between a single counterion and individual charged surfaces, i.e.,

$$W_1 = -\frac{qe_0\sigma_1}{2\varepsilon\varepsilon_0}\left(\frac{D}{2}+z\right), \quad W_2 = -\frac{qe_0\sigma_2}{2\varepsilon\varepsilon_0}\left(\frac{D}{2}-z\right). \tag{68}$$

Since in the strong-coupling regime the free energy is given *via* simple quadratures, it is much simpler to evaluate it than on the weak-coupling level. Defining the rescaled free energy
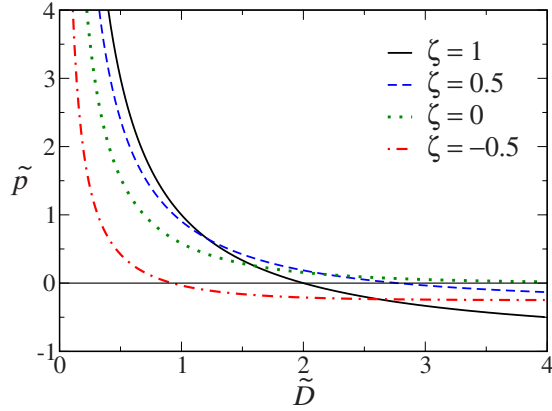
FIG. 3. (Color online) Rescaled strong-coupling intersurface pressure, Eq. (71), as a function of the rescaled distance, $\tilde{D}$, between two charged plates for different asymmetry parameters ζ $=-0.5$, 0, 0.5, and 1 as shown on the graph. Long-distance attractive pressure is suppressed for the $\zeta=0$ case. For symmetrically charged surface ($\zeta=1$), we recover the standard SC result $\tilde{p}(\tilde{D})=-1+2/\tilde{D}$ [9].

$$\widetilde{\mathcal{F}} = \frac{2\varepsilon\varepsilon_0}{\sigma_1^2 \mu^3} \mathcal{F}, \qquad (69)$$

we obtain

$$\frac{\widetilde{\mathcal{F}}}{\widetilde{S}} = (1 + \zeta^2)\frac{\tilde{D}}{2} - (1 + \zeta)\ln \sinh\left((1 - \zeta)\frac{\tilde{D}}{2}\right). \qquad (70)$$

Differentiating the free energy with respect to the surface-surface distance $\tilde{D}$ we get the corresponding pressure acting between the bounding surfaces

$$\tilde{p}(\tilde{D}) = -\frac{1}{2}(1 + \zeta^2) + \frac{1}{2}(1 - \zeta^2)\coth\left((1 - \zeta)\frac{\tilde{D}}{2}\right). \quad (71)$$

The dependence of this dimensionless pressure on the separation for different values of ζ is presented in Fig. 3. Note that the SC pressure can become attractive for both like-charged and oppositely charged surfaces which contrasts with the mean-field theory that does not allow attraction between like-charged surfaces. This is because of the strong electrostatic correlations mediated by counterions between the charged surfaces for $\Xi \gg 1$ and has been investigated thoroughly before for equally charged surfaces [9]. Our results show that a similar attraction mechanism holds for asymmetrically charged surfaces in the SC limit.

The pressure exhibits two well-defined limiting laws obtainable for small and large inter-surface separations. For small separations $\tilde{D} \ll 1$, we have

$$\tilde{p}(\tilde{D}) \simeq \frac{1 + \zeta}{\tilde{D}}, \qquad (72)$$

for arbitrary $|\zeta| < 1$ as noted in Sec. II. For large separations $\tilde{D} \gg 1$, we obtain
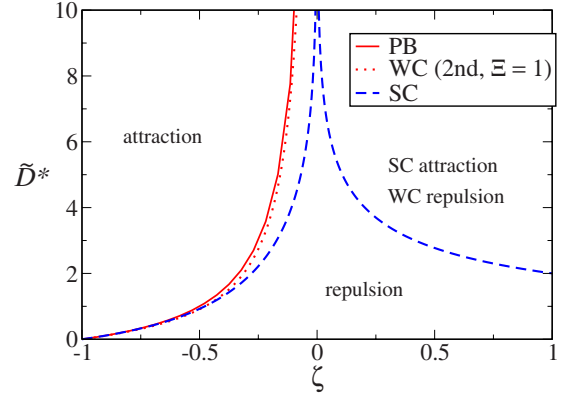

FIG. 4. (Color online) Rescaled bound-state surface-surface separation $\tilde{D}^* = 2\tilde{a}^*$ as a function of the asymmetry parameter ζ as predicted by the zeroth-order PB theory (solid line), Eq. (34), the second-order WC theory at $\Xi = 1$ (dotted line), and the strong-coupling theory (dashed line), Eq. (74). Surfaces attract for $\tilde{D} > \tilde{D}^*$ and repel otherwise. Only in the SC limit can two surfaces of equal sign ($\zeta > 0$) attract. The second-order WC result is obtained by finding the zero-pressure point of the total WC pressure $\tilde{p}(\tilde{D})$ $= \tilde{p}_0(\tilde{D}) + \tilde{p}_2(\tilde{D})$, Eq. (43), for given Ξ and ζ.

$$\tilde{p}(\tilde{D}) \simeq -\zeta^2. \qquad (73)$$

Note that in the limit $\tilde{D} \to 0$ the SC pressure coincides with the PB result on the leading order [compare Eqs. (21) and (72)] and represents the ideal-gas osmotic pressure of counterions which dominates over the electrostatic contributions. The PB and SC forms for $\zeta < 0$ coincide also in the limit of $\tilde{D} \gg 1$ [compare Eqs. (31) and (73)] and reduce to the pressure in the capacitor.

The dependence of the pressure on the intersurface separation points to the existence of a bound state defined *via* $p(D^*) = 0$. The SC bound-state separation D^* can be expressed analytically as

$$\tilde{D}^* = -\frac{2 \ln|\zeta|}{1 - \zeta}, \qquad (74)$$

and is presented in Fig. 4 as a function of ζ. Obviously both like-charged and oppositely charged surfaces can form bound states at small surface-surface separations. The bound-state separation approaches infinity and the surfaces unbind asymptotically as $\zeta \to 0$, that is when one plate becomes electroneutral.

Finally one can also derive the explicit form of the counterion density as a function of the normal coordinate z. This can be read off simply from the integrand in Eq. (66), that is $n(z) = C \exp[-\beta(W_1 + W_2)]$, where C is a normalization factor [5,9]. According to the electroneutrality condition, we normalize the density as $\int_{-a}^{a} n(z)dz = -(\sigma_1 + \sigma_2)/qe_0$, or in rescaled units,

$$\int_{-\tilde{a}}^{\tilde{a}} \tilde{n}(\tilde{z}) d\tilde{z} = 1 + \zeta, \tag{75}$$

where we have defined $\tilde{z} = z/\mu$ with $\mu = -e_0/(2\pi\ell_B q\sigma_1)$ being the Gouy-Chapman length with respect to plate 1. From here, the density profile is obtained as

$$\tilde{n}(z) = \frac{1 - \zeta^2}{2} \frac{e^{-(1-\zeta)\tilde{z}}}{\sinh[(1-\zeta)\tilde{D}/2]}, \tag{76}$$

as a function of z and ζ.

Regime of validity of the strong-coupling theory. The regime of applicability of the leading order SC theory follows from a simple criterion that has been discussed and confirmed previously in the case of equally charged surfaces by both MC simulations and higher-order calculations [4,5,9]. The generalization to asymmetrically charged surfaces is straightforward.

For large couplings, counterions are strongly attracted to an oppositely charged surface as the counterion-surface interaction becomes large and equivalently, the Gouy-Chapman length, μ, and the thickness of the counterionic layer at the surface become small. The layer thickness must be compared with the typical lateral spacing between counterions $a_\perp$. For counterions sandwiched between two asymmetrically charged surfaces, this latter quantity follows from the local electroneutrality condition as

$$a_\perp^2 \simeq -\frac{\sigma_1 + \sigma_2}{qe_0}, \tag{77}$$

up to a factor of the order unity and assuming that the surfaces are sufficiently close so that they may be strongly coupled *via* the counterions as will be determined consistently here. In rescaled units, one gets

$$\tilde{a}_\perp^2 \simeq (1 + \zeta)\Xi, \tag{78}$$

where $\tilde{a}_\perp = a_\perp/\mu$. Obviously, $\tilde{a}_\perp$ becomes large relative to the layer thickness as Ξ grows. Note that on the other hand, the lateral Coulomb repulsion between counterions in this quasi-two-dimensional layer becomes much larger than the thermal energy, i.e., $q^2\ell_B/a_\perp \sim \sqrt{\Xi} \gg 1$, indicating that counterions form a strongly correlated liquid in which they are highly localized within correlation holes of lateral size $\tilde{a}_\perp \sim \sqrt{\Xi} \gg 1$ [4,5,9]. Thus for surface-surface separations, $\tilde{D}$, smaller than the correlation hole size, i.e.,

$$\tilde{D} \ll \sqrt{(1+\zeta)\Xi}, \tag{79}$$

counterions can move almost independently from each other in the direction normal to the surface and one can safely assume that the effective surface-surface interaction as well as the counterionic density profile follow only from the interactions of individual counterions with the bounding charged surfaces. The counterion-counterion interactions contribute on the subleading order and matter at larger separations. This picture is of course confirmed on a systematic level by the SC expansion analysis [4,5,9], and the above equation sets a criterion for the validity regime of the single-

particle leading-order SC theory ($\Xi \to \infty$), when applied to finite coupling parameters.

VII. SIMULATIONS

We performed Monte Carlo (MC) simulations in order to study the system of two asymmetrically charged surfaces beyond the analytical limits of weak and strong coupling discussed above. All simulations were performed in the Canonical ensemble (NVT) using the standard Metropolis algorithm [40]. The mobile counterions were modeled as point charges [33] enclosed in a simulation box bounded in the z direction by two charged surfaces of distance D and surface charge densities σ_1 and σ_2 (compare Fig. 1). Periodic boundary conditions were applied in the lateral directions parallel to the bounding surfaces. The lateral size of the charged surfaces, L, which is set equal to the lateral size of the simulation box, was held fixed throughout all the simulations. The number of counterions, N, was varied between 60 and 1800, depending on the system parameters in order to fulfill the electroneutrality condition. The counterions interact through the Coulombic potential

$$U(r_{ij}) = \frac{q_i q_j}{4\pi\varepsilon\varepsilon_0 r_{ij}}, \tag{80}$$

with $q_i = e_0 q$ being the charge of the ith counterion and r_{ij} the separation distance between the ith and the jth counterions (with $i,j = 1, \ldots, N$). The interaction energy of the ith counterion with the charged surfaces in the simulation box are given by

$$U_k(z_{ik}) = \frac{q_i \sigma_k}{4\pi\varepsilon\varepsilon_0} \left\{ 4L \ln \frac{\sqrt{L^2/2 + z_{ik}^2} + L/2}{\sqrt{(L/2)^2 + z_{ik}^2}} \right.$$
$$\left. - 2z_{ik} \left[\arcsin\left(\frac{(L/2)^4 - z_{ik}^4 - (L^2/2)z_{ik}^2}{[(L/2)^2 + z_{ik}^2]^2} \right) + \frac{\pi}{2} \right] \right\}, \tag{81}$$

where $\sigma_k = \sigma_1$ and σ_2 is surface charge density of the kth surface (with $k = 1,2$) and z_{ik} is the normal distance between the ith counterion and the kth surface. The long-ranged Coulomb interactions in this system were accounted for *via* a charged sheet scheme similar to that proposed by Torrie and Valleau [41]. This scheme makes use of the counterion profile in the simulation box in order to calculate an external field, stemming from the long-ranged interactions. This external field is iteratively updated and self-consistency is achieved normally in a few iterations.

In the course of simulations, new configurations were created by trial displacements of the counterions and equilibration was accomplished by running through 10^6 configurations. The 10^7 following configurations were then used for the production runs.

The pressure p was calculated in the production runs according to the contact-value theorem as

$$p_k = k_B T n_k^{\text{contact}} - \frac{\sigma_k^2}{2\varepsilon\varepsilon_0}, \qquad (82)$$

where n_k^{contact} is the density of counterions at contact with the kth surface. In thermodynamic equilibrium, the pressure does not depend on which surface ($k=1$ or $k=2$) is chosen in order to calculate the pressure from the above equation, and the contact condition at both surfaces leads to precisely the same value for the pressure. All simulations were conducted at fixed temperature $T=298$ K, lateral simulation box size $L=245$ Å, and dielectric constant $\varepsilon=78.7$, which is assumed to be the same throughout the system.

The simulations were performed at different values of the coupling parameter Ξ and the asymmetry parameter ζ. We explored the Ξ parameter space extensively by using $\Xi=0.32, 0.64, 2.5, 3.2, 5.1, 6.4, 8.6, 17, 25, 51, 86,$ and 172 in order to cover exhaustively both the weak-coupling and the strong-coupling regimes. The concurrent values of the asymmetry parameter were always taken as $\zeta=-0.5, 0, +0.5$ at each value of the coupling parameter. The results are plotted in the form of rescaled density and pressure as previously defined in this paper (Sec. III).

VIII. DISCUSSION

In order to assess the validity of the weak- and strong-coupling results presented above for asymmetrically charged surfaces, we performed extensive MC simulations and compared them to analytical results in both limits. It transpires from this comparison that the simulation results corresponding to an exact evaluation of the partition function are always bracketed by the WC and the SC limiting forms, smoothly approaching them in the appropriate limits of the coupling parameter Ξ.

First we compare the density profiles of simulations with theoretical results given by Eqs. (20) and (30) for the PB limit and Eq. (76) for the SC limit (solid and dashed lines in Fig. 5, respectively). As seen from Fig. 5 the theoretical PB and SC rescaled density profiles represent two extremal cases and all MC simulations results with finite values of Ξ are located consistently between these two limits. The MC results for small Ξ are almost exactly spot on the PB prediction, while larger discrepancies are observed as Ξ grows. For large enough $\Xi > 10$, the MC results slowly converge to the SC result. This is especially clear for surfaces with charges of equal sign, $\zeta=0.5$, whereas for surfaces with opposite sign, $\zeta=-0.5$, there is no big difference between PB and SC profiles.

Next we consider the intersurface pressure as obtained from the simulations (symbols in Fig. 6) as well as the PB theory, Eqs. (19) and (29), and the SC theory, Eq. (71) (solid and dashed lines, respectively). The PB result is expected to be valid for separations $\tilde{D} \gg \Xi$ [9] (see also Sec. V C). Therefore, for $\Xi=0.32$ the PB line expectedly agrees nicely with the simulation data (open squares) in the whole range of separations shown in the figure. Upon closer inspection, however, we find small deviations from the PB result as shown in the insets in Fig. 6 for all three values of the asymmetry parameter ζ. In this case, the fluctuation correction to
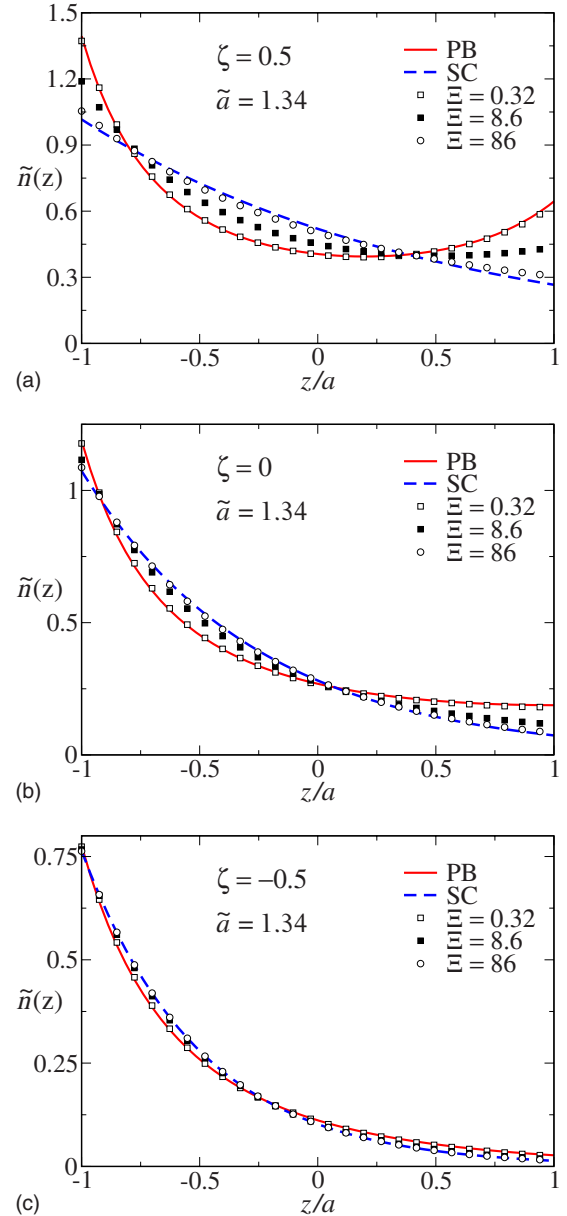

FIG. 5. (Color online) Rescaled counterion density profile $\tilde{n}(z)$ between two asymmetrically charged surfaces at half-separation $\tilde{a} = \tilde{D}/2 = 1.34$ for three different asymmetry parameters $\zeta=0.5$, 0, and -0.5 (top to bottom). Solid lines represent the PB prediction, Eqs. (20) and (30), and the dashed lines show the SC prediction, Eq. (76). Symbols correspond to MC simulations data at three different coupling parameters $\Xi=0.32$ (open squares), 8.6 (filled squares), and 86 (open circles).

the mean-field pressure accurately compensates for these deviations and adding the second-order correction to the PB pressure leads to a total WC pressure, Eq. (43) (shown as a dotted line in the inset) that matches the simulation data perfectly. Note that the pressure changes can be drastic even on the WC level as ζ assumes different values. For $\zeta=0.5$ and 0 the WC pressure is strictly repulsive, while it turns attractive and leads to a bound state (zero pressure point) for $\zeta=-0.5$.
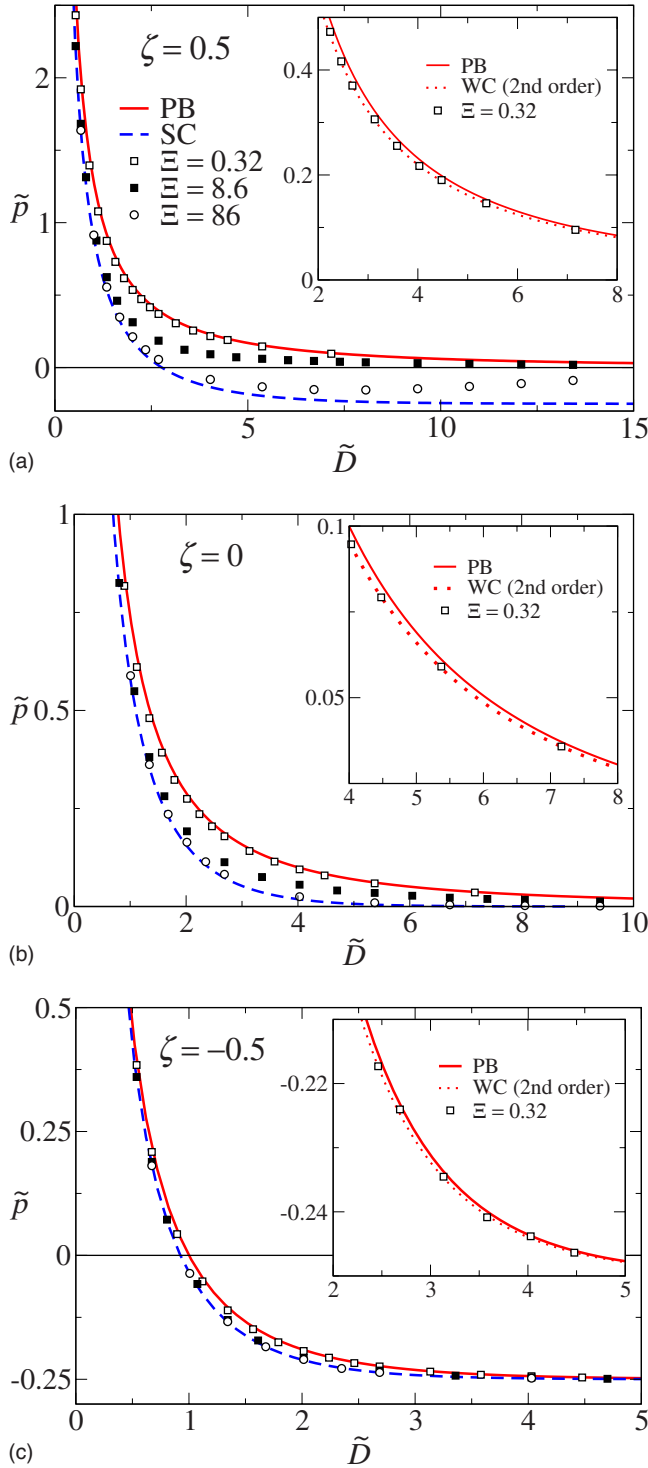
FIG. 6. (Color online) Rescaled interaction pressure, $\tilde{p}$, as a function of the rescaled intersurface distance, $\tilde{D}$, for three different values of the asymmetry parameter $\zeta = 0.5$, 0 and -0.5 (top to bottom). Solid lines represent the PB prediction, Eqs. (19) and (29), dotted lines show the second-order weak-coupling pressure (PB plus second-order corrections), Eq. (43), and the dashed lines are the SC prediction, Eq. (71). Symbols correspond to MC simulations data at three different coupling parameters $\Xi = 0.32$ (open squares), 8.6 (filled squares), and 86 (open circles). Insets show details at small pressures along with the PB theory result as well as the second-order WC result for $\Xi = 0.32$.

In the intermediate regime of coupling parameters, the simulation results for the pressure are clearly bracketed by the two limiting analytical forms, given by the PB plus the second-order correction and the SC expressions of the interaction pressure. The SC prediction is expected to be valid for separations $\tilde{D} \ll \sqrt{\Xi}$ as discussed in Sec. VI. Consistently, the interaction pressure starts off close to the strong-coupling limit at small separations and then smoothly converges to the weak-coupling limit for larger separations. This is strictly true for $\zeta = 0.5$ and 0. In the case of $\zeta = -0.5$ the difference between the strong- and weak-coupling results for the rescaled interaction pressure is marginal and the simulation data and the analytical results nearly coincide for all rescaled separations $\tilde{D} = D/\mu$. We emphasize that the pressures and the density profiles are plotted here in rescaled representation; in actual units, Fig. 6 corresponds to different ranges of separation, D, for the WC and SC regimes as the Gouy-Chapman length, μ, is typically very different between the two limits (small at high couplings and large at small couplings as may be realized, e.g, by changing the counterion valency at fixed surface charge densities and Bjerrum length).

For large values of the coupling parameter the simulation results for the interaction pressure expectedly follow very closely the strong-coupling prediction for a wider range of intersurface separations. The correspondence between the SC theory and simulations is better for $\zeta = -0.5$ than for $\zeta = 0.5$, which can be again traced back to the fact that the strong- and weak-coupling results are very close to one another for charged surfaces of opposite sign in the whole range of rescaled separations, whereas they differ significantly in the case of surfaces of equal sign. For intermediate and large couplings, we have not attempted to compare our data with the second-order WC approximation as this approximation breaks down at the range of distances shown in the figures (Sec. V C).

Note also that in all cases considered here the theoretical and the simulated values of the interaction pressure converge for very small surface-surface separations. In fact, the SC and PB results coincide in the leading order as the rescaled distance, $\tilde{D}$, tends to zero, Eqs. (21) and (72), since both are dominated by the osmotic pressure of counterions. The subleading corrections for very small $\tilde{D}$ are different in the PB and SC limits and on this level the simulation data with finite Ξ are generally expected to agree better with the SC prediction at small separations [9].

We now consider the simulated bound-state separation, D^*, as a function of the coupling parameter in Fig. 7 (symbols). For $\zeta = 0.5$, the PB theory ($\Xi \to 0$) gives only repulsion and predicts no bound state. While the SC theory predicts a closely packed bound state with D^* given by Eq. (74), explicitly here $\tilde{D}^* \simeq 2.77$. As seen, by increasing the coupling parameter the simulation data for D^* (filled squares) decrease monotonically and rather slowly converge to the SC prediction (dotted line). The comparison is again worse for the $\zeta = 0.5$ than for the $\zeta = -0.5$ case (dashed line and filled circles). For $\zeta = 0.5$, even at $\Xi = 86$ the difference between the simulations and the analytical result is still close to 10%. The deviations are quite pronounced for smaller values of the
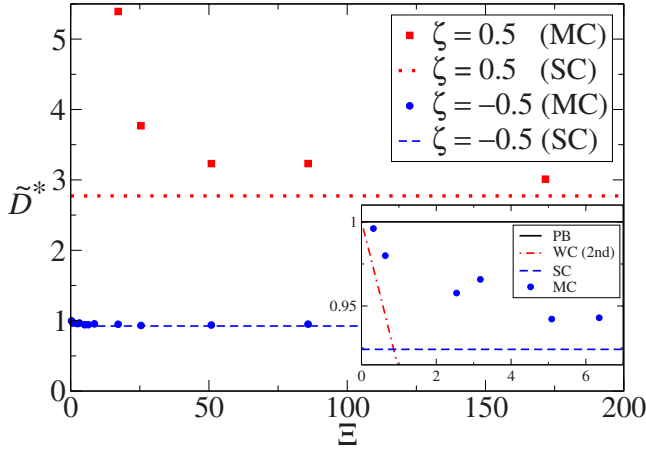
FIG. 7. (Color online) Rescaled bound-state separation $\widetilde{D}^*$ as a function of the coupling parameter Ξ for different values of ζ. Main set: Symbols are simulation data for $\zeta=0.5$ (filled squares) and -0.5 (filled circles). The SC results, Eq. (74), for $\zeta=-0.5$ and 0.5 are represented by dashed and dotted lines, respectively. The inset represents the detailed view for $\zeta=-0.5$, where we also show the zeroth-order PB result, Eq. (34) (solid line), and the result from the second-order WC approximation (dotted-dashed line) obtained numerically from Eq. (43).

coupling parameter. The opposite is true for $\zeta=-0.5$. Here, the simulation results are close to the strong-coupling analytical limit in the whole range of Ξ values. For $\Xi<4$ we can discern, see inset in Fig. 7, weak-coupling behavior that starts off with the PB-predicted value $\widetilde{D}^*=1$ in the limit of $\Xi\to0$ [Eq. (34), solid line], that later follows the PB plus second-order corrections line (dotted-dashed line) and then rapidly approaches the strong-coupling result $\widetilde{D}^*\simeq0.92$ (dashed line). As already noted the differences between strong and weak coupling in this case are marginal in the rescaled representation.

The dependence of $\widetilde{D}^*$ on ζ in Fig. 8 complements the above observations. The bound-state separation diverges for $\zeta=0$ both in simulations as well as in the analytical limits. Here we reproduce the simulation results at $\zeta=0.5$ and -0.5, which again clearly show the convergence to the SC result for $\zeta=0.5$ and the crossover from the PB result (solid line) to the SC result (dashed line) for $\zeta=-0.5$ upon increasing the coupling parameter. The quantitative agreement between the simulations and the analytical results in the two limiting cases of PB and SC is excellent. Note here again that the second-order WC expansion (dotted line in the inset) begins to fail at small separations as it deviates from the limiting PB results as well as from the simulation data. Since the PB pressure is zero on the PB phase boundary line, the validity of the second-order WC correction can be assessed analytically only by performing a two-loop calculation which goes beyond the scope of this paper.

IX. CONCLUSIONS

To summarize, we have derived theoretical forms for the interaction pressure as well as the counterionic density pro-
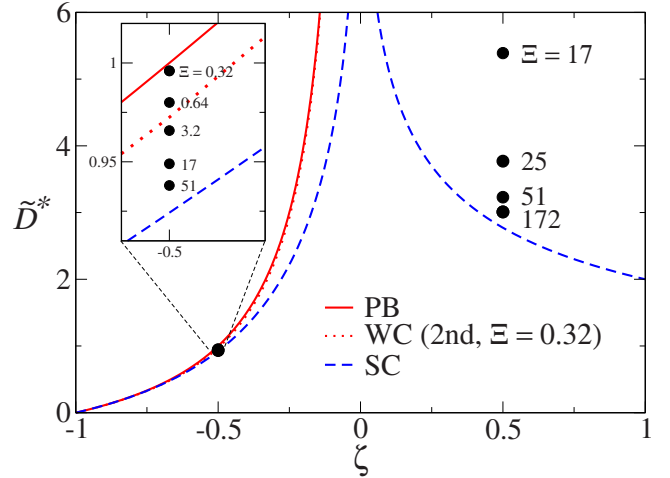

FIG. 8. (Color online) Rescaled bound-state separation $\widetilde{D}^*$ as a function of ζ. Symbols are simulation data for different values of the coupling parameter at $\zeta=0.5$ and -0.5. The region around $\zeta=-0.5$ is expanded in the inset showing the crossover from the PB prediction (solid line) to the SC prediction (dashed line) upon increasing the coupling parameter.

files of asymmetrically charged planar surfaces with neutralizing counterions in between. Based on the field-theoretical methods we analyzed two different regimes of weak and strong coupling as defined by the electrostatic coupling parameter Ξ. The crossover between these two regimes is studied *via* Monte Carlo simulations.

For small values of Ξ, the system is described very well by the weak-coupling (WC) theory, that in the lowest (zeroth) order coincides with the mean-field Poisson-Boltzmann (PB) result. The second order of WC corresponds to a first-order loop expansion and represents the contribution from correlated quadratic fluctuations around the mean-field or saddle-point solution. This second-order correction, which is proportional to Ξ, always lowers the interaction pressure between the surfaces and thus leads to an attractive contribution to the total interaction pressure. Since it corresponds to an expansion of the partition function around the mean-field saddle point it must be smaller, in absolute terms, than the mean-field result. Net attraction given by the second-order fluctuations term (for interacting surfaces of equal sign) is therefore inconsistent with the nature of the WC approximation.

For large values of the coupling parameter Ξ, the weak-coupling approach breaks down and the virial expansion amounting to the strong-coupling (SC) approximation must be used. The SC approach is effectively a one-particle theory and takes properly into account the strong correlation and interaction of the counterions with external surface fields on the leading order [9]. Following standard procedures, we derived an analytical expression for interaction pressure in the SC limit. The interaction pressure in this case is always lower than the PB result and can be negative (corresponding to a net attractive force) even for charged surfaces of equal sign.

We compared both our theories, i.e., WC with second-order corrections and SC, with Monte Carlo simulations. We

found very good agreement for both theories in their expected regime of validity. As expected, the WC approach is valid for separations $\tilde{D} \gg \Xi$. The second-order correction improves the small discrepancies between PB and MC results at large separations but it tends to fail for smaller distances when discrepancies get more pronounced. On the other hand, the SC theory describes the behavior perfectly at small separations $\tilde{D} \ll \sqrt{\Xi}$. For small enough coupling parameter Ξ, the validity of the PB approximation spreads to smaller separations, $\tilde{D}$, where PB and SC results nearly coincide (in the rescaled representation). Therefore, we may conclude that for sufficiently small Ξ, the PB result is valid on the whole interval $\tilde{D}$.

Note that the second-order WC contribution to the interaction pressure consistently diverges (toward large negative values) for small intersurface separations, $\tilde{D} < 1$, irrespective of ζ, which makes it in general inapplicable in this limit. The reason for this is simple. For small intersurface separations the mean-field solution becomes more and more homogeneous, almost a constant, and the second-order interaction free energy approaches its standard zero-frequency van der Waals form that diverges for small separations.

In the case of surface charges with equal sign, $\zeta > 0$, the WC theory predicts no attraction and hence no bound state. The attraction and the corresponding bound state appear only for coupling parameters Ξ that are large enough, as predicted by the SC theory. In the case of charged surfaces of opposite sign, $\zeta < 0$, the attraction appears also in the WC limit above a threshold value $\tilde{D}^*$ that represents the equilibrium surface-surface separation.

It is notable that for charged surfaces of opposite sign, the WC analysis in general performs much better than for the surfaces of equal sign and that the SC and the WC results are very close to one another for charged surfaces of opposite sign in the whole range of rescaled separations, whereas they differ significantly in the case of surfaces of equal sign. There is also only a marginal difference between the PB and SC counterion density profiles in the rescaled representation for surfaces of opposite sign. A reasonable explanation for this would be in our opinion that for oppositely charged surfaces the counterions mostly feel the effect of the strong uniform external field provided by the surface charges, which acts similarly in the strong-coupling limit as well as the weak-coupling limit. Thus the mean-field and the strong coupling approaches should converge. In the case of similarly charged surfaces, the mean-field theory depends more on the local counterion density whereas the strongly coupled counterions still feel mostly the external field, be it uniform or nonuniform. Thus, we have the difference between the WC and the SC frameworks in the $\zeta < 0$ and $\zeta > 0$ cases.

Our results support an emerging paradigm, according to which the WC and the SC limit bracket the exact results for the interaction pressure between charged surfaces neutralized by mobile counterions. They indeed provide quantitatively correct results for the interaction pressure in the limit of small and large intersurface separations, while at intermediate separations the exact results are always located between the two limits. It thus seems advisable that in analyzing the electrostatic interactions in colloidal systems one always calculates both analytic limits, the WC as well as the SC, in order to get a good handle on the range of values that the interaction can assume for any value of the electrostatic coupling parameter. In the future we intend to study the same system in the presence of added salt and dielectric discontinuities.

[1] *Electrostatic Effects in Soft Matter and Biophysics*, edited by C. Holm, P. Kekicheff, and R. Podgornik (Kluwer Academic, Dordrecht, 2001).

[2] *Soft Condensed Matter Physics in Molecular and Cell Biology*, edited by W. C. K. Poon and D. Andelman (Taylor and Francis, New York, London, 2006).

[3] E. J. Verwey and J. G. Overbeek, *Theory of the Stability of Lyophobic Colloids* (Elsevier, Amsterdam, 1948).

[4] H. Boroudjerdi, Y. W. Kim, A. Naji, R. R. Netz, X. Schlagberger, and A. Serr, Phys. Rep. **416**, 129 (2005).

[5] A. Naji, S. Jungblut, A. G. Moreira, and R. R. Netz, Physica A **352**, 131 (2005).

[6] I. Rouzina and V. A. Bloomfield, J. Phys. Chem. **100**, 9977 (1996).

[7] A. Y. Grosberg, T. T. Nguyen, and B. I. Shklovskii, Rev. Mod. Phys. **74**, 329 (2002).

[8] Y. Levin, Rep. Prog. Phys. **65**, 1577 (2002).

[9] R. R. Netz, Eur. Phys. J. E **5**, 557 (2001); A. G. Moreira and R. R. Netz, *ibid.* **8**, 33 (2002).

[10] Y. Burak, D. Andelman, and H. Orland, Phys. Rev. E **70**, 016102 (2004).

[11] C. D. Santangelo, Phys. Rev. E **73**, 041512 (2006).

[12] M. M. Hatlo and L. Lue, e-print arXiv:0806.3716v1.

[13] L. Guldbrand, B. Jönsson, H. Wennerström, and P. Linse, J. Chem. Phys. **80**, 2221 (1984).

[14] D. Bratko, B. Jönsson, and H. Wennerström, Chem. Phys. Lett. **128**, 449 (1986).

[15] J. P. Valleau, R. Ivkov, and G. M. Torrie, J. Chem. Phys. **95**, 520 (1991).

[16] R. Kjellander, T. Åkesson, B. Jönsson, and S. Marčelja, J. Chem. Phys. **97**, 1424 (1992).

[17] Y.-G. Chen and J. D. Weeks, Proc. Natl. Acad. Sci. U.S.A.

103, 7560 (2006); J. M. Rodgers, C. Kaur, Y.-G. Chen, and J. D. Weeks, Phys. Rev. Lett. **97**, 097801 (2006).

[18] Y. S. Jho, G. Park, C. S. Chang, P. A. Pincus, and M. W. Kim, Phys. Rev. E **73**, 021502 (2006).

[19] M. Trulsson, B. Jönsson, T.Åkesson, J. Forsman, and C. Labbez, Phys. Rev. Lett. **97**, 068302 (2006); Langmuir **23**, 11562 (2007).

[20] R. Podgornik and B. Žekš, J. Chem. Soc., Faraday Trans. 2 **84** 611 (1988); R. Podgornik, J. Phys. A **23**, 275 (1990).

[21] P. Attard, J. Mitchell, and B. W. Ninham, J. Chem. Phys. **88**, 4987 (1988).

[22] M. Kardar and R. Golestanian, Rev. Mod. Phys. **71**, 1233 (1999).

[23] R. R. Netz and H. Orland, Eur. Phys. J. E **1**, 203 (2000).

[24] P. A. Pincus and S. A. Safran, Europhys. Lett. **42**, 103 (1998).

[25] A. W. C. Lau and P. Pincus, Phys. Rev. E **66**, 041501 (2002).

[26] B.-Y. Ha, Phys. Rev. E **64**, 031507 (2001).

[27] V. A. Parsegian and D. Gingell, Biophys. J. **12**, 1192 (1972).

[28] A. W. C. Lau and P. Pincus, Eur. Phys. J. B **10**, 175 (1999).

[29] D. Ben-Yaakov, Y. Burak, D. Andelman, and S. A. Safran, Europhys. Lett. **79**, 48002 (2007).

[30] S. A. Safran, Europhys. Lett. **69**, 826 (2005).

[31] A. A. Meier-Koll, C. C. Fleck, and H. H. von Grünberg, J. Phys.: Condens. Matter **16**, 6041 (2004).

[32] P. Sens and J.-F. Joanny, Phys. Rev. Lett. **84**, 4862 (2000).

[33] In our model excluded-volume counterion-counterion repulsions are neglected. These two-body interactions will be irrelevant in the leading order within the strong-coupling limit [4,5]. However, the counterion size (or the counterion-wall excluded-volume interactions) is incorporated exactly by taking $D=2a$ as the closest-approach surface-surface distance leaving out the counterion diameter from the actual distance. On a more fundamental level it is indeed possible to incorporate excluded-volume effects within a modifed Poisson-Boltzmann formulation as in, e.g., I. Borukhov, D. Andelman, and H. Orland, Phys. Rev. Lett. **79**, 435 (1997); Electrochim. Acta **46**, 221 (2000).

[34] O. Punkkinen, A. Naji, R. Podgornik, I. Vattulainen, and P.-L. Hansen, Europhys. Lett. **82**, 48001 (2008).

[35] Y. S. Jho, G. Park, C. S. Chang, P. A. Pincus, and M. W. Kim, Phys. Rev. E **76**, 011920 (2007).

[36] M. Kanduč and R. Podgornik, Eur. Phys. J. E **23**, 265 (2007).

[37] Y. S. Jho, M. Kanduč, A. Naji, R. Podgornik, M. W. Kim, and P. A. Pincus, Phys. Rev. Lett. **101**, 188101 (2008).

[38] R. R. Netz, Eur. Phys. J. E **3**, 131 (2000); R. Menes, P. Pincus, and B. Stein, Phys. Rev. E **62**, 2981 (2000); J. Schmit, R. Menes, and P. A. Pincus, *ibid.* **66**, 061502 (2002); M. M. Hatlo, R. A. Curtis, and L. Lue, J. Chem. Phys. **128**, 164717 (2008).

[39] P. Ziherl, R. Podgornik, and S. Žumer, Chem. Phys. Lett. **295**, 99 (1998).

[40] N. A. Metropolis, A. W. Rosenbluth, M. N. Rosenbluth, A. Teller, and E. Teller, J. Chem. Phys. **21**, 1087 (1953).

[41] G. M. Torrie and J. P. Valleau, J. Phys. Chem. **86**, 3251 (1982).